

Quantum information scrambling in the presence of weak and strong thermalization

Zheng-Hang Sun,^{1,2} Jian Cui,^{3,*} and Heng Fan^{1,2,4,†}

¹*Institute of Physics, Chinese Academy of Sciences, Beijing 100190, China*

²*School of Physical Sciences, University of Chinese Academy of Sciences, Beijing 100190, China*

³*Department of Physics, Key Laboratory of Micro-Nano Measurement-Manipulation and Physics (Ministry of Education), Beihang University, Beijing 100191, China*

⁴*Songshan Lake Materials Laboratory, Dongguan 523808, Guangdong, China*

Quantum information scrambling under many-body dynamics is of fundamental interest. The tripartite mutual information can quantify the scrambling via its negative value. Here, we first study the quench dynamics of tripartite mutual information in a non-integrable Ising model where the strong and weak thermalization are observed with different initial states. We numerically show that the fastest scrambling can occur when the energy density of the chosen initial state possesses the maximum density of states. We then present an experimental protocol for observing weak and strong thermalization in a superconducting qubit array. Based on the protocol, the relation between scrambling and thermalization revealed in this work can be directly verified by superconducting quantum simulations.

I. INTRODUCTION

Under unitary dynamics, whether or not the locally encoded quantum information is delocalized and spreads over the entire system is a fundamental problem [1, 2]. When delocalization of quantum information occurs in a system, it is referred to a scrambler. One prominent example as such is black hole, which is revealed as the most efficient scrambler [3–5]. The characterization of scramblers attracts considerable attention [6–8]. A well-known probe of quantum information scrambling is the out-of-time-order correlator (OTOC), whose decay rate extracted from its dynamics is closely related to the Lyapunov exponent [6, 9]. Quantum information scrambling can provide insight into the subjects in condensed-matter physics. By studying the OTOCs, it has been recognized that the scrambling plays an important role in information propagation [10, 11], many-body localization (MBL) transitions [12–14], and quantum phase transitions [15–18].

Besides the OTOC, the scrambling can also be characterized by the negative tripartite mutual information (TMI) [6, 7]. Different from the OTOC, the TMI is an operator-independent quantity. The experimental measurements of OTOCs and TMI require different technologies. The direct measurement of OTOCs requires the inverse-time evolution, which can be performed in trapped ions [19] and nuclear magnetic resonance (NMR) quantum simulators [20]. Nevertheless, the inverse-time evolution is an experimental challenge in quantum superconducting circuits because of the local intra-qubit interactions [21]. On the other hand, to measure the TMI, the

quantum state tomography (QST) should be employed. The accurate and efficient QST can be performed in several platforms, such as trapped ions [22], superconducting qubits [21, 23–25] and NMR [26]. Consequently, TMI is an experimentally feasible quantity in general.

Recently, more attention has been paid to the TMI in many-body quantum systems. It has been shown that the TMI can diagnose the ergodic and MBL phase, i.e., the TMI is close to 0 and the scrambling is suppressed in the MBL phase, while the TMI becomes smaller in the ergodic phase indicating faster scrambling [27]. In addition, the scrambling is observed in both Bethe integrable system with fermionic interactions and a generic non-integrable system. In contrast, one-dimensional non-interacting fermions do not scramble [28].

Previous studies of the TMI mainly focused on its dependence on the integrability of the system. In fact, the dynamics of a quantum system is also determined by the choice of initial state. A paradigm in this regard is the weak and strong thermalization [29]. Starting from an initial state corresponding to the Gibbs state with inverse temperature β far away from 0, it has been revealed that the dynamics shows obviously persistent oscillation, which is a signature of weak thermalization. However, if one chooses an initial state with $\beta \simeq 0$, strong thermalization can be observed. The weak and strong thermalization in a non-integrable Ising model with both parallel and longitude magnetic fields was numerically explored [29, 30], and explained from a quasiparticle view point [31]. Recent numerical results of long-range Ising model suggest the existence of weak and strong thermalization in this system, paving the way to experimentally observing the phenomena in trapped ions [32].

In this work, we first study the time evolution of TMI in the non-integrable Ising model with different initial states, and reveal the relation between the information

* jianCui@buaa.edu.cn

† hfan@iphy.ac.cn

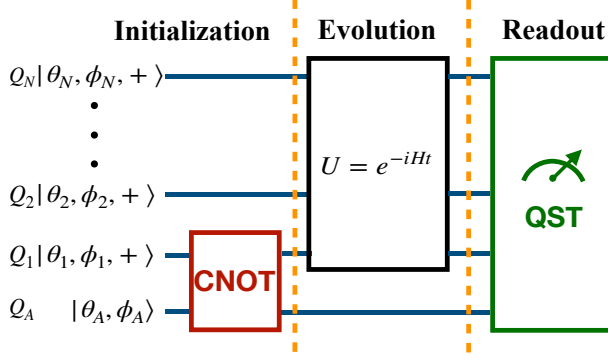


FIG. 1. Schematic representation of the generic experimental protocol for studying quantum information scrambling by measuring the TMI. The sequence consists of three parts: (i) Initialization. (ii) Evolution. (iii) Readout. Through out the protocol, the whole system remains in pure state.

scrambling and the degree of thermalization. We then present an experimental protocol for observing weak and strong thermalization in a superconducting qubit array, which is one of the most popular superconducting circuit. Finally, we calculate the TMI in the superconducting qubit array, showing the relation between information scrambling and thermalization can be experimentally demonstrated on a superconducting qubit array.

II. RESULTS

A. Tripartite mutual information and a generic experimental protocol

Before the calculation of TMI, three subsystems \mathcal{A} , \mathcal{B} , and \mathcal{C} should be chosen, and the remainder is the subsystem \mathcal{D} . The reduced density matrices of the subsystems \mathcal{A} , \mathcal{B} , \mathcal{C} , and \mathcal{D} are denoted as $\rho_{\mathcal{A}}$, $\rho_{\mathcal{B}}$, $\rho_{\mathcal{C}}$, and $\rho_{\mathcal{D}}$, respectively. The definition of TMI is [6]

$$I_3 = S(\rho_{\mathcal{A}}) + S(\rho_{\mathcal{B}}) + S(\rho_{\mathcal{C}}) + S(\rho_{\mathcal{D}}) - S(\rho_{\mathcal{AB}}) - S(\rho_{\mathcal{AC}}) - S(\rho_{\mathcal{BC}}), \quad (1)$$

where $S(\rho) = -\text{Tr}(\rho \log \rho)$ is the von Neumann entropy. A negative value far away from zero is a diagnostic of quantum information scrambling [6].

We then present a generic experimental protocol for studying quantum information scrambling by measuring the TMI. Fig. 1 is a schematic diagram of the protocol. The system is comprised of N qubits denoted as Q_1, Q_2, \dots , and Q_N , and an ancillary qubit Q_A (see Fig. 1). We define the state $|\theta, \phi, \pm\rangle$ as the eigenstate of the matrix $\hat{n} \cdot \vec{\sigma} = (\sin \theta \cos \phi) \sigma^x + (\sin \theta \sin \phi) \sigma^y + (\cos \theta) \sigma^z$ (σ^α with $\alpha \in \{x, y, z\}$ referring to the Pauli matrices) with

the eigenvalues ± 1 . The initial state of Q_A is $|\theta_A, \phi_A\rangle \equiv (|\theta_1, \phi_1, +\rangle + |\theta_1, \phi_1, -\rangle)/\sqrt{2}$. The generalized CNOT gate in Fig. 1 reads

$$\text{CNOT} \equiv |\theta_1, \phi_1, +\rangle \langle \theta_1, \phi_1, +| \otimes \mathbf{1} + |\theta_1, \phi_1, -\rangle \langle \theta_1, \phi_1, -| \otimes \tilde{X}, \quad (2)$$

where $\mathbf{1}$ is a two-dimensional identity matrix, and $\tilde{X} \equiv R\sigma^x R^{-1}$ with

$$R \equiv \begin{pmatrix} \cos \frac{\theta_1}{2} & -e^{-i\phi_1} \sin \frac{\theta_1}{2} \\ e^{i\phi_1} \sin \frac{\theta_1}{2} & \cos \frac{\theta_1}{2} \end{pmatrix}. \quad (3)$$

After applying the CNOT gate, we in fact generate a two-qubit GHZ state $|\text{GHZ}\rangle_{A1} = (|\theta_1, \phi_1, +\rangle_A |\theta_1, \phi_1, +\rangle_1 + |\theta_1, \phi_1, -\rangle_A |\theta_1, \phi_1, -\rangle_1)/\sqrt{2}$, entangling the ancillary qubit and Q_1 and locally encoding the information in the two qubits. In short, the initial state can be written as

$$|\psi_0\rangle = |\text{GHZ}\rangle_{A1} (\otimes_{j=2}^N |\theta_j, \phi_j, +\rangle). \quad (4)$$

Actually, when we chose $\theta_i = 0$ or π , the aforementioned initialization is the same as the one employed in Ref. [27]. This initialization is enlightened by the thought experiment for the retrieval of quantum information from a black hole [3].

The next step is the time evolution under the quantum channel $U = e^{-iHt}$ with H as the Hamiltonian of the N -qubits isolated system. To study the quantum information scrambling, we conventionally consider the spin chains that are beyond quadratic fermionic form after the Jordan-Wigner transformation [28]. The final step is measuring the TMI by QST based on Eq. (2). We choose $\mathcal{A} = Q_A$, $\mathcal{B} = Q_1$, $\mathcal{C} = \{Q_2, Q_3, \dots, Q_{N/2}\}$, where N is even for convenience, and the reminder as the subsystem \mathcal{D} . The protocol can quantify how the locally encoded information scrambles through quantum dynamics.

B. Results for a non-integrable Ising model

We first consider a spin-1/2 Ising model whose Hamiltonian reads

$$H_{\text{Ising}} = -J \sum_{i=1}^{N-1} \sigma_i^z \sigma_{i+1}^z + g \sum_{i=1}^N \sigma_i^x + h \sum_{i=1}^N \sigma_i^z \quad (5)$$

with g and h referring to the strength of the transverse and the parallel magnetic field. When $g \cdot h \neq 0$, the Ising model is non-integrable. We fix $g/J = 1.05$ and $h/J = -0.5$. Similar to the quench protocol in Ref. [29], the chosen initial states are isotropic, i.e., $\theta = \theta_i$ and $\phi = \phi_i \forall i \in \{1, 2, \dots, N\}$ in Eq. (4), and $|\theta, \phi\rangle \equiv \otimes_{i=1}^N |\theta_i, \phi_i, +\rangle$. The inverse temperature β for the state $|\theta, \phi\rangle$ can be obtained by solving the equation $\text{Tr}\{[\rho(\beta) - \rho(\theta, \phi)]H\} = 0$

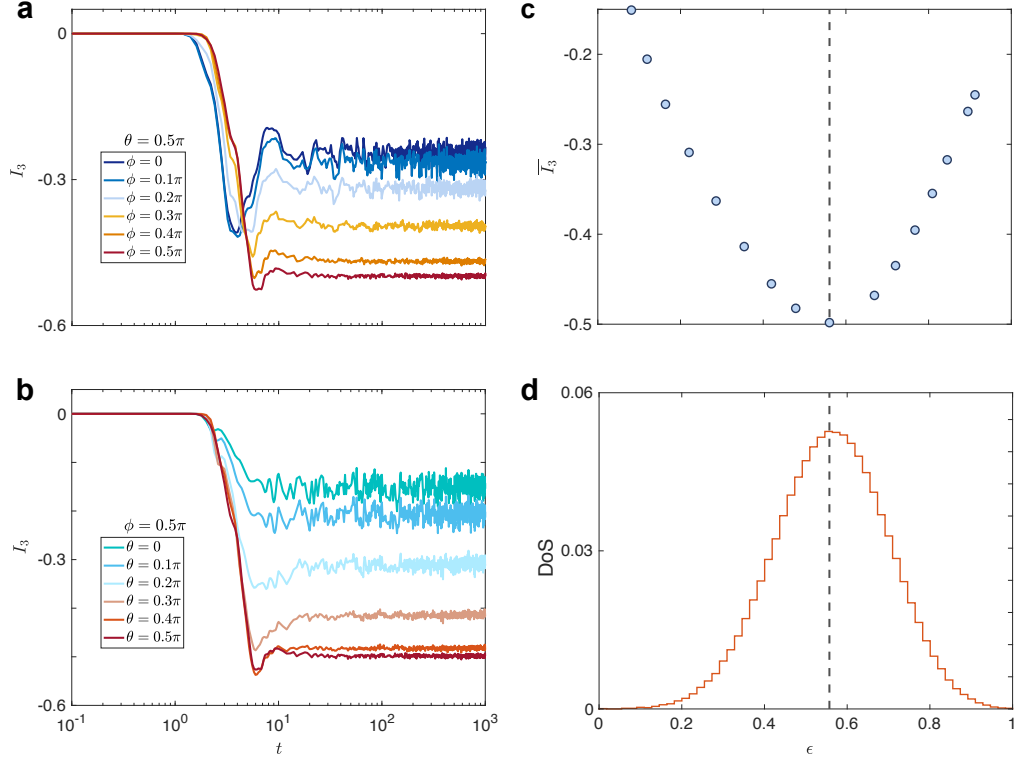


FIG. 2. Panel **a** and **b** show the dynamics of the TMI with different isotropic initial states $|\theta, \phi\rangle$. The time-averaged TMI and the density of state (DoS) as a function of the energy density ϵ are depicted in the panel **c** and **d**, respectively.

with $\rho(\theta, \phi) \equiv |\theta, \phi\rangle\langle\theta, \phi|$, $\rho(\beta) \equiv e^{-\beta H} / \text{Tr}(e^{-\beta H})$, and H as the Hamiltonian.

It has been shown that the quench dynamics with the initial state $|Z+\rangle = |0, \phi, +\rangle$ (i.e., $\beta \simeq 0.7275$) shows a signature of weak thermalization, while with $|Y+\rangle = |\pi/2, \pi/2, +\rangle$ (i.e., $\beta = 0$) as the initial state, strong thermalization occurs [29]. Additionally, we can employ the energy density

$$\epsilon = \frac{\langle\theta, \phi, +|H|\theta, \phi, +\rangle - E_{\min}}{E_{\max} - E_{\min}} \quad (6)$$

with $E_{\max(\min)}$ as the maximum (minimum) eigenvalue of the Hamiltonian H . The energy density can quantify the relative position of the state in the energy spectrum. It can be directly calculated that for $|Z+\rangle$ in the weak thermalization regime, the energy density $\epsilon \simeq 0.0812$, i.e., $|Z+\rangle$ is quite close to the ground state of H_{Ising} (Here, the system size is $N = 14$), which is consistent with the quasiparticle explanation in Ref. [31]. However, the energy density of $|Y+\rangle$ is $\epsilon \simeq 0.5602$, far away from the ground state. We emphasize that the state $|X+\rangle = |\pi/2, 0, +\rangle$ ($\beta \simeq -0.7180$ and $\epsilon \simeq 0.9122$) lies in a rare region where local observables depart from their thermal values during the time evolution and no thermalization is observed [29].

Using the protocol in Fig. 1, we study the quench dynamics of TMI I_3 with several isotropic initial states parameterized by θ and ϕ in H_{Ising} with system size $N = 14$. We first demonstrate that even in the absence of thermalization, information scrambling characterized by $I_3 < 0$ can still be observed (see the result in Fig. 2a with $\theta = 0.5\pi$ and $\phi = 0$), indicating that the occurrence of negative I_3 is independent of thermalization. Nevertheless, when ϕ ranges from 0 to 0.5π , the decrease of TMI suggests that stronger thermalization corresponds to faster information scrambling (see Fig. 2a). Figure 2b presents the dynamics of I_3 with $\phi = 0.5\pi$ and $\theta \in [0, 0.5\pi]$, and shows a similar tendency of TMI in Fig. 2a.

To further understand the dependence of scrambling on initial states, we consider a time-averaged TMI $\overline{I_3} \equiv \frac{1}{t_f - t_i} \int_{t_i}^{t_f} I_3(t) dt$ with $t_i = 100$ and $t_f = 1000$, extracting the stationary value of TMI from its dynamics. The energy density ϵ can characterize the initial states in strong or weak thermalization regime, and therefore we plot the $\overline{I_3}$ as a function of ϵ in Fig. 2c. There is a local minimum $\overline{I_3}$ near $\epsilon \simeq 0.56$, which exactly corresponds to a maximum density of states (DoS) (Fig. 2d), revealing that the most efficient scrambling occurs when the initial state has the energy density with maximal DoS.

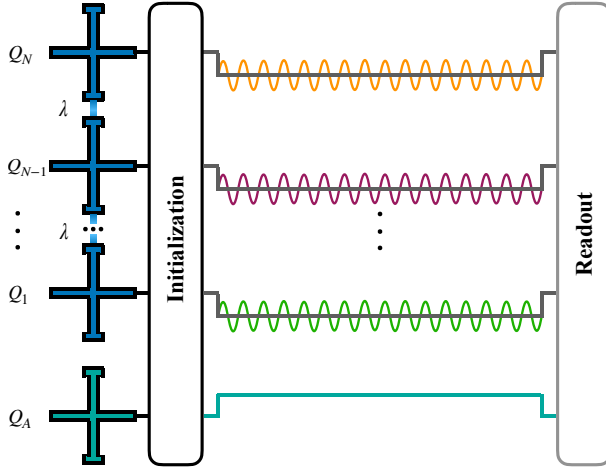


FIG. 3. Schematic representation of the experimental waveform sequence for the time evolution. The qubit Q_1, Q_2, \dots, Q_N are biased to the interaction frequency ω_q^{int} via their Z pulse control lines (the rectangular pulses). Since the ancillary qubit Q_A does not participate in the time evolution, its frequency should be detuned away from ω_q^{int} . Meanwhile, the microwave drives (the sinusoidal pulses) are imposed on Q_1, Q_2, \dots, Q_N through the XY-control lines.

As a side remark, we compare the dynamics of TMI for different initial isotropic states with the same energy density ϵ , and for the initial Néel-type and the isotropic states with the same ϵ . The results are presented in Supplementary Note 1, showing that the stationary values of TMI are almost identical for all initial states with the same ϵ .

C. Experimental protocol for observing weak and strong thermalization on a superconducting qubit array

The one-dimensional spin-1/2 XY model

$$H_{XY} = \lambda \sum_{i=1}^{N-1} (\sigma_i^x \sigma_{i+1}^x + \sigma_i^y \sigma_{i+1}^y) \quad (7)$$

can be typically realized by a chain of transmon qubits with capacitive couplings λ [21, 33–35]. The Hamiltonian H_{XY} can be mapped to a free fermion system via the Jordan-Wigner transformation [36]. Thus, it is well-known that thermalization is absent in H_{XY} because of the infinitely many conserved quantities in thermodynamic limit (for a finite XY chain, there are extensive number of conserved quantities) [37–39]. To make the superconducting qubit array non-integrable for observing quantum thermalization, we impose uniform resonant microwave drives on all qubits, generating the local transverse field with amplitude Ω , and the final Hamiltonian

reads (see Methods for details)

$$H_{\text{SQA}} = \lambda \sum_{i=1}^{N-1} (\sigma_i^x \sigma_{i+1}^x + \sigma_i^y \sigma_{i+1}^y) + \Omega \sum_{i=1}^N \sigma_i^y. \quad (8)$$

The local transverse field has been realized in a recent quantum simulation experiment [40], where the XY-crosstalk correction and phase alignment of the transverse field were discussed. A sketch of the pulse sequence for the realization of the Hamiltonian (8) is depicted in Fig. 3.

Before we study the TMI in the Hamiltonian (8), the weak and strong thermalization in the system should be demonstrated. Here, we adopt $\lambda = \Omega = 1$ and $N = 14$. It can be calculated that for the isotropic initial state $|\theta, \phi\rangle = |\pi/2, 1.369\pi\rangle$, the inverse temperature $\beta \simeq 0$, and the strong thermalization is expected. To observe the weak thermalization, we consider another isotropic initial state $|\pi/2, 0.369\pi\rangle$ with $\beta \simeq -0.6547$. Moreover, we recognize that the energy of a typical initial state $|Z+\rangle$ is $\langle Z+ | H_{\text{SQA}} | Z+\rangle = 0$. Thus, for $|Z+\rangle$, $\beta = 0$, and $|Z+\rangle$ lies in the strong thermalization regime. In supplementary Note 2, we show that the dynamical properties of H_{SQA} with the initial state $|Z+\rangle$ are similar to those with the initial state $|\pi/2, 1.369\rangle$.

Similar to Ref. [29], we pay attention to the quench dynamics of local observables $\langle O(t) \rangle - \langle O \rangle_{\text{th}}$ with $O \in \{\sigma^x, \sigma^y, \sigma^z\}$, and the operator norm distance between a reduced density matrix (RDM) of a three-body subsystem and the corresponding thermal density matrix denoted as $d(\rho^{\text{sub.}}(t), \rho_{\text{th}}^{\text{sub.}})$ (see Methods for the detailed definitions). The time evolution of local observables with two different initial states are shown in Fig. 4a and b. One can see that the values of the observables relax to the thermal values when the initial state is $|\theta, \phi\rangle = |\pi/2, 1.369\pi\rangle$ ($\beta \simeq 0$) and in the strong thermalization region. However, the undamped oscillation of $\langle O(t) \rangle - \langle O \rangle_{\text{th}}$ can be observed with another initial state $|\theta, \phi\rangle = |\pi/2, 0.369\pi\rangle$, which is a signature of the weak thermalization. Moreover, figure 4c shows the dynamics of $d(\rho^{\text{sub.}}(t), \rho_{\text{th}}^{\text{sub.}})$ with the two initial states. In the strong thermalization region, the quenched RDM fast saturates to the thermal state and the distance $d(\rho^{\text{sub.}}(t), \rho_{\text{th}}^{\text{sub.}})$ monotonically decays, while the distance exhibits dramatic fluctuation in the weak thermalization region.

D. Results for the superconducting qubit array

We then study the TMI I_3 in the Hamiltonian (8). Figure 4d presents the time evolution of I_3 with the two initial states. The behaviors of I_3 are similar to those in the Ising model (see Fig. 2a and d). Fast and slow quantum information scrambling are observed in the strong

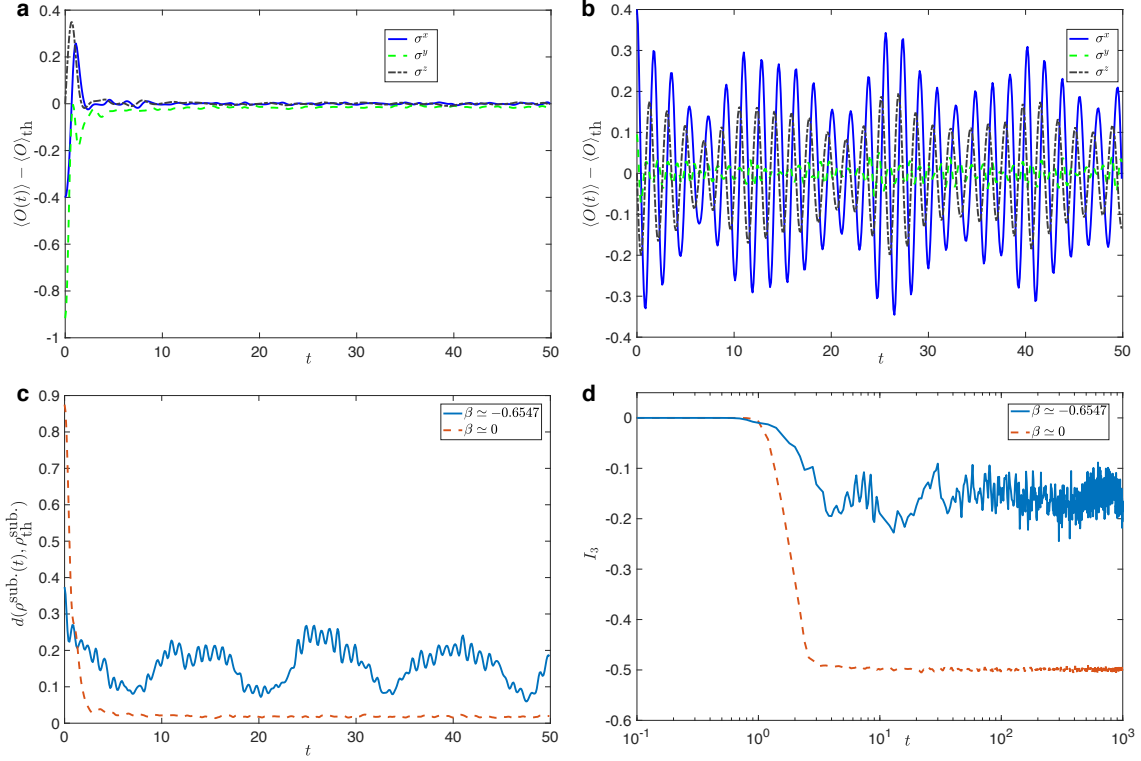


FIG. 4. Panel **a** and **b** show the dynamics of local observables with the initial state $|\theta, \phi\rangle = |\pi/2, 1.369\pi\rangle$ ($\beta \approx 0$) and $|\theta, \phi\rangle = |\pi/2, 0.369\pi\rangle$ ($\beta \approx -0.6547$), respectively. Panel **c** shows the distance $d(\rho^{\text{sub.}}(t), \rho_{\text{th}}^{\text{sub.}})$ with the two initial states. Panel **d** shows the dynamics of the TMI I_3 with the two initial states.

and weak thermalization region, respectively. Moreover, the saturation of I_3 at long time can also be observed in the system (8).

Next, we study the relation between the TMI and the energy density ϵ . Different from the Ising model (5), the minimum attainable ϵ of all isotropic states is 0.3093 in the system (8) (see Supplementary Information Note 1). To study the I_3 of the initial states with $\epsilon < 0.3093$, we can consider the Néel-type initial states (see Supplementary Information Note 1). Figure 5a depicts the time-averaged TMI $\bar{I}_3 \equiv \frac{1}{t_f - t_i} \int_{t_i}^{t_f} I_3(t) dt$ ($t_i = 100$ and $t_f = 1000$) as a function of ϵ . We also present the DoS of the Hamiltonian (8) as a function of ϵ in Fig. 5b. The comparison between Fig. 5a and b indicates that the fastest information scrambling occurs when the initial state has the ϵ with maximum DoS. The results of I_3 in the Hamiltonian (8) suggest that the linkage between information scrambling and thermalization revealed in the Ising model (5) can be experimentally verified in the superconducting qubit array using the aforementioned protocol.

III. DISCUSSION

We have investigated the quantum information scrambling in the systems where the strong and weak thermalization exist. The occurrence of information scrambling quantified by the negative TMI, i.e., $I_3 < 0$, can be observed in both strong and weak thermalization regimes. Ref. [29] indicates the absence of quantum thermalization for the initial state $|X+\rangle$ in the Ising model (5). However, our result in figure 2a shows information scrambling during its quench dynamics with the initial state $|X+\rangle$. Actually, it has been pointed out that scrambling does not equal quantum thermalization [27, 41], and our results are consistent with the viewpoint. Nevertheless, the existence of no thermalization region in the Ising model remains an open question due to the two numerical challenges. Firstly, the matrix product state (MPS) algorithm can only simulate short-time evolution [29], while one has to compute long-time dynamics reaching thermalization time to obtain more solid evidence. Secondly, a recent numerical work using MPS combined with Chebyshev polynomial expansions shows there are significantly large error bars of the results for the states

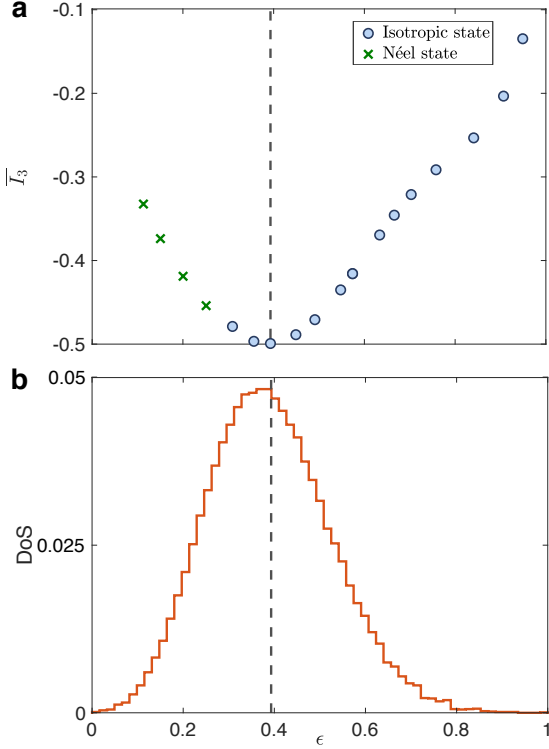


FIG. 5. For the Hamiltonian (8), the time-averaged TMI and the density of state (DoS) as a function of the energy density ϵ are depicted in the panel **a** and **b**, respectively.

in the no thermalization region since the states are close to the edge of the DoS spectrum [42]. In Supplementary Note3, we present a finite-size analysis of the no thermalization region employing the Lanczos-Krylov space-time calculations, suggesting that the results of the infinite system in Ref. [29] support the finite-size results.

We reveal that the value of I_3 is closely related to the weak and strong thermalization characterized via the energy density and DoS. Ref. [32] reveals the weak and strong thermalization in the long-range Ising model, which can be realized in tapped-ion quantum simulator [43]. As a consequence, this work may inspire the investigations on the quantum information scrambling in long-range interacting systems [44], especially in the presence of weak and strong thermalization [32]. Besides the weak thermalization, the weak ergodicity breaking characterized by the long-lived oscillations can also be originated from quantum many-body scars [45, 46], and the study of information scrambling with quantum many-body scars is another intriguing direction to explore in the future.

Quantum thermalization dynamics has been experimentally studied in optical lattice [47] and tapped ions [48]. Previous experiments mainly focus on the

strong thermalization (which is actually regarded as the conventional quantum thermalization), and a distinct comparison between weak and strong thermalization remains absent. We develop a scheme to probe weak and strong thermalization in a superconducting qubit array, and the results can be readily demonstrated in quantum simulation experiments.

It has been shown that the energy density plays a key role in the MBL mobility edge [49–52]. The relation between information scrambling and energy density revealed by our work could provide new insight into the mobility edge. Furthermore, the slow information scrambling in the weak thermalization region has potential applications for quantum information storage devices [25] and stabilizing out-of-equilibrium phases of matter [53, 54].

IV. METHODS

A. Realization of the Hamiltonian (8) in a superconducting qubit array

Conventionally, the Hamiltonian of a transmon qubit array can be described by the Bose-Hubbard model [21, 25]

$$H_{\text{BH}} = \Lambda \sum_{i=1}^{N-1} (a_i^\dagger a_{i+1} + a_i a_{i+1}^\dagger) + \frac{U}{2} \sum_{i=1}^N n_i(n_i - 1) \quad (9)$$

with a_i^\dagger (a_i) as the bosonic creation (annihilation) operator, $n_i = a_i^\dagger a_i$, U as strength of nonlinear interaction and Λ referring to the nearest hopping strength. In the limit $U/\Lambda \rightarrow \infty$, the Hamiltonian (9) reduces to a XY model [55, 56]

$$\begin{aligned} H_{XY} &= \Lambda \sum_{i=1}^{N-1} (\sigma_i^+ \sigma_{i+1}^- + \sigma_i^- \sigma_{i+1}^+) \\ &= \lambda \sum_{i=1}^{N-1} (\sigma_i^x \sigma_{i+1}^x + \sigma_i^y \sigma_{i+1}^y) \end{aligned} \quad (10)$$

with $\lambda = \Lambda/2$.

Actually, the non-equilibrium properties of the Bose-Hubbard model (9) are close to those of the XY model (10) when $U/\Lambda \geq 8$ [56]. For the device in Ref. [21], $U/\Lambda \simeq 18$, and the XY model can be experimentally studied using analog quantum simulation.

When the microwave drives with amplitude Ω are applied to each qubit, we can obtain [57]

$$H_{\text{drive}} = \Omega \sum_{j=1}^N e^{-i\varphi_j} \sigma_j^+ + e^{i\varphi_j} \sigma_j^-. \quad (11)$$

By adjusting the phase of the microwave drives, one can force $\varphi = \varphi_j = \pi/2$ ($j = 1, 2, \dots, N$), and then H_{drive} can

be rewritten as $H_{\text{drive}} = \Omega \sum_{j=1}^N \sigma_j^y$. Thus, the Hamiltonian (8), i.e., $H_{\text{SQA}} = H_{XY} + H_{\text{drive}}$ can be realized in a qubit array.

To better understand the strong thermalization in the system (8), we can rewrite the Hamiltonian in the σ^x basis

$$H_{\text{SQP}} = \Lambda \sum_{i=1}^{N-1} \sigma_i^z \sigma_{i+1}^z + \Omega \sum_{i=1}^N \sigma_i^x + \Omega \sum_{i=1}^{N-1} \sigma_i^x \sigma_{i+1}^x \quad (12)$$

$$= H_0 + H_{\text{int.}}$$

By employing the Jordan-Wigner transformation $\sigma_i^x = 1 - 2c_i^\dagger c_i$ and $\sigma_i^z = -\prod_{l<i} (1 - 2c_l^\dagger c_l)(c_i + c_i^\dagger)$ with c_i^\dagger (c_i) referring to the fermionic creation (annihilation) operator, one can see that in the Hamiltonian (12), $H_0 \equiv \Lambda \sum_{i=1}^{N-1} \sigma_i^z \sigma_{i+1}^z + \Omega \sum_{i=1}^N \sigma_i^x$ as the Ising model without parallel field can be regarded as a quadratic system (free fermions). Moreover, the $H_{\text{int.}} \equiv \Omega \sum_{i=1}^{N-1} \sigma_i^x \sigma_{i+1}^x$ gives the Heisenberg coupling $c_i c_i c_{i+1} c_{i+1}$, from which the quantum thermalization and MBL are originated [58]. Based on above discussions, we explain the occurrence of the strong thermalization in the superconducting qubit array.

B. The quantities employed to quantify the quantum thermalization

Here, we briefly introduce the definitions of the quantities that quantify the quantum thermalization. During the quench dynamics, there exists an exchange of infor-

mation from a small subsystem \mathcal{A} to the complementary one $\bar{\mathcal{A}}$ that acts as a thermal bath of \mathcal{A} . The reduced density operator of \mathcal{A} at time t is $\rho^{\mathcal{A}}(t) \equiv \text{Tr}_{\bar{\mathcal{A}}} \{\rho(t)\}$ with $\rho(t)$ as the quenched state. The thermal density matrix of the same system equilibrium at temperature T is $\rho_{\text{th.}}(T) = Z^{-1} \exp(-\beta H)$ with $\beta = 1/T$ as the inverse temperature and $Z \equiv \text{Tr} \{\exp(-\beta H)\}$, and thus $\rho_{\text{th.}}^{\mathcal{A}} \equiv \text{Tr}_{\bar{\mathcal{A}}} \{\rho_{\text{th.}}(T)\}$. When the quantum thermalization occurs, with a long time t and a temperature T , $\rho^{\mathcal{A}}(t) = \rho_{\text{th.}}^{\mathcal{A}}(T)$ [59].

As a direct consequence, if a quantity can measure the distance between $\rho^{\mathcal{A}}(t)$ and $\rho_{\text{th.}}^{\mathcal{A}}(T)$, it can be employed to quantify the quantum thermalization. In Ref. [29] and our work, two quantities are considered. The first one is related to the local observables, whose definition is

$$\langle \mathcal{O}(t) \rangle - \langle \mathcal{O} \rangle_{\text{th.}} = \text{Tr} \{ \mathcal{O} (\rho^{\mathcal{A}}(t) - \rho_{\text{th.}}^{\mathcal{A}}(T)) \}, \quad (13)$$

where \mathcal{O} is the local observables $\sum_{i=1}^N \sigma_i^\alpha / N$ ($\alpha \in \{x, y, z\}$). The second one is the distance $d(\rho^{\mathcal{A}}(t), \rho_{\text{th.}}^{\mathcal{A}}(T))$ defined as the maximum eigenvalue of the matrix $\rho^{\mathcal{A}}(t) - \rho_{\text{th.}}^{\mathcal{A}}(T)$. In this work, we chose the subsystem \mathcal{A} consisting of the qubit Q_5 , Q_6 and Q_7 .

ACKNOWLEDGMENTS

We acknowledge the enlightening discussion with M. C. Bañuls. This work was supported by NSFC (Grant Nos. 11904018, 11774406, 11934018), National Key R&D Program of China (Grant Nos. 2016YFA0302104, 2016YFA0300600), Strategic Priority Research Program of Chinese Academy of Sciences (Grant No. XDB28000000), and Beijing Academy of Quantum Information (Grant No. Y18G07).

-
- [1] Lewis-Swan, R.J., Safavi-Naini, A., Kaufman, A.M. & Rey, A. M. Dynamics of quantum information. *Nat. Rev. Phys.* **1**, 627-634 (2019).
 - [2] Eisert, J., Friesdorf, M. & Gogolin, C. Quantum many-body systems out of equilibrium. *Nat. Phys.* **11**, 124-130 (2015).
 - [3] Hayden, P. & Preskill, J. Black holes as mirrors: Quantum information in random subsystems. *J. High Energy Phys.* **09**, 120 (2007).
 - [4] Sekino, Y. & Susskind, L. Fast scramblers. *J. High Energy Phys.* **10**, 065 (2008).
 - [5] Maldacena, J., Shenker, S. H. & Stanford, D. A bound on chaos. *J. High Energy Phys.* **08**, 106 (2016).
 - [6] Hosur, P., Qi, X.-L., Roberts, D. A. & Yoshida, B. Chaos in quantum channels. *J. High Energy Phys.* **02**, 004 (2016).
 - [7] Sünderhalf, C., Piroli, L., Qi, X.-L., Schuch, N. & Cirac, J. I. Quantum chaos in the Brownian SYK model with large finite N : OTOCs and tripartite information. *J. High Energy Phys.* **11**, 038 (2019).
 - [8] Nakagawa, Y. O., Sárosi, G. & Ugajin, T. Chaos and relative entropy. *J. High Energy Phys.* **07**, 002 (2018).
 - [9] Swingle, B. Unscrambling the physics of out-of-time-order correlators. *Nat. Phys.* **14**, 988-990 (2018).
 - [10] Luitz, D. J. & Lev, Y. B. Information propagation in isolated quantum systems. *Phys. Rev. B* **96**, 020406(R) (2017).
 - [11] Huang, Y., Zhang, Y.-L. & Chen, X. Out-of-time-ordered correlators in many-body localized systems. *Ann. Phys. (Berlin)* **529**, 1600318 (2017).
 - [12] He, R.-Q. & Lu, Z.-Y. Characterizing many-body localization by out-of-time-ordered correlation. *Phys. Rev. B* **95**, 054201 (2017).
 - [13] Sahu, S., Xu, S. & Swingle, B. Scrambling Dynamics across a Thermalization-Localization Quantum Phase Transition. *Phys. Rev. Lett.* **123**, 165902 (2019).
 - [14] Chen, X., Zhou, T., Huse, D. A. & Fradkin, E. Out-of-time-order correlations in many-body localized and ther-

- mal phases. *Ann. Phys. (Berlin)* **529**, 1600332 (2017).
- [15] Sun, Z.-H., Cai, J.-Q., Tang, Q.-C., Hu, Y. & Fan, H. Out-of-Time-Order Correlators and Quantum Phase Transitions in the Rabi and Dicke Models. *Ann. Phys. (Berlin)* **532**, 1900270 (2020).
- [16] Shen, H., Zhang, P., Fan, R. & Zhai, H. Out-of-time-order correlation at a quantum phase transition. *Phys. Rev. B* **96**, 054503 (2017).
- [17] Dağ, C. B., Sun, K. & Duan, L.-M. Detection of Quantum Phases via Out-of-Time-Order Correlators. *Phys. Rev. Lett.* **123**, 140602 (2019).
- [18] Wei, B.-B., Sun, G. & Hwang, M.-J. Dynamical scaling laws of out-of-time-ordered correlators. *Phys. Rev. B* **100**, 195107 (2019).
- [19] Gärtner, M., Bohnet, J., Safavi-Naini, A., Wall, M. L., Bollinger, J. J. & Rey, A. M. Measuring out-of-time-order correlations and multiple quantum spectra in a trapped-ion quantum magnet. *Nat. Phys.* **13**, 781-786 (2017).
- [20] Li, J., Fan, R., Wang, H., Ye, B., Zeng, B., Zhai, H., Peng, X. & Du, J. Measuring Out-of-Time-Order Correlators on a Nuclear Magnetic Resonance Quantum Simulator. *Phys. Rev. X* **7**, 031011 (2017).
- [21] Yan, Z. et al. Strongly correlated quantum walks with a 12-qubit superconducting processor. *Science* **364**, 753-756 (2019).
- [22] Jurcevic, P. et al. Direct Observation of Dynamical Quantum Phase Transitions in an Interacting Many-Body System. *Phys. Rev. Lett.* **119**, 080501 (2017).
- [23] Xu, K. et al. Emulating many-body localization with a superconducting quantum processor. *Phys. Rev. Lett.* **120**, 050507 (2018).
- [24] Neill, C. et al. Ergodic dynamics and thermalization in an isolated quantum system. *Nat. Phys.* **12**, 1037-1041 (2016).
- [25] Chiaro, B. et al. Growth and preservation of entanglement in a many-body localized system. ArXiv: 1910.06024.
- [26] Li, K. et al. Measuring holographic entanglement entropy on a quantum simulator. *npj Quantum Inf.* **5**, 30 (2019).
- [27] Iyoda, E. & Sagawa, T. Scrambling of quantum information in quantum many-body systems. *Phys. Rev. A* **97**, 042330 (2018).
- [28] Schnaack, O., Bölter, N., Paeckel, S., Manmana, S. R., Kehrein, S. & Schmitt, M. *Phys. Rev. B* **100**, 224302 (2019).
- [29] Bañuls, M. C., Cirac, J. I. & Hastings, M. B. Strong and Weak Thermalization of Infinite Nonintegrable Quantum Systems. *Phys. Rev. Lett.* **106**, 050405 (2011).
- [30] Hastings, M. B. & Mahajan, R. Connecting Entanglement in Time and Space: Improving the Folding Algorithm. *Phys. Rev. A* **91**, 032306 (2015).
- [31] Lin, C.-J. & Motrunich, O. I. Quasiparticle explanation of the weak-thermalization regime under quench in a non-integrable quantum spin chain. *Phys. Rev. A* **95**, 023621 (2017).
- [32] Liu, F., Lundgren, R., Titum, P., Pagano, G., Zhang, J., Monroe, C. & Gorshkov, A. V. Confined Quasiparticle Dynamics in Long-Range Interacting Quantum Spin Chains. *Phys. Rev. Lett.* **122**, 150601 (2019).
- [33] Wendin, G. Quantum information processing with superconducting circuits: a review. *Reports Prog. Phys.* **80**, 106001 (2017).
- [34] Risté, D. et al. Detecting bit-flip errors in a logical qubit using stabilizer measurements. *Nat. Commun.* **6**, 6983 (2015).
- [35] Chen, Y. et al. Qubit Architecture with High Coherence and Fast Tunable Coupling. *Phys. Rev. Lett.* **113**, 220502 (2014).
- [36] Lieb, E., Schultz, T. & Mattis, D. Two soluble models of an antiferromagnetic chain. *Ann. Phys.* **16**, 407-466 (1961).
- [37] Rigol, M., Dunjko, V., Yurovsky, V. & Olshanii, M. Relaxation in a completely integrable many-body quantum system: an ab initio study of the dynamics of the highly excited states of 1d lattice hard-core bosons. *Phys. Rev. Lett.* **98**, 050405 (2007).
- [38] Biroli, G., Kollath, C. & Läuchli, A. M. Effect of rare fluctuations on the thermalization of isolated quantum systems. *Phys. Rev. Lett.* **105**, 250401 (2010).
- [39] Nakagawa, Y. O., Watanabe, M., Fujita, H. & Sugiura, S. Universality in volume-law entanglement of scrambled pure quantum states. *Nat. Commun.* **9**, 1635 (2018).
- [40] Xu, K. et al. Probing dynamical phase transitions with a superconducting quantum simulator. *Sci. Adv.* **6**, eaba4935 (2020).
- [41] Xu, T., Scaffidi, T. & Cao, X. Does scrambling equal chaos? *Phys. Rev. Lett.* **124**, 140602 (2020).
- [42] Yang, Y., Iblisdir, S., Cirac, J. I. & Bañuls, M. C. Probing thermalization through spectral analysis with matrix product operators. *Phys. Rev. Lett.* **124**, 100602 (2020).
- [43] Monroe, C. et al. Programmable Quantum Simulation of Spin Systems with Tapped Ions. ArXiv: 1912.07845.
- [44] Pappalardi, S., Russomanno, A., Žunkovič, B., Iemini, F., Silva, A. & Fazio, R. Scrambling and entanglement spreading in long-range spin chains. *Phys. Rev. B* **98**, 134303 (2018).
- [45] Bernien, H. et al. Probing many-body dynamics on a 51-atom quantum simulator. *Nature* **551**, 579-584 (2017).
- [46] Turner, C. J., Michailidis, A. A., Abanin, D. A., Serbyn, M. & Papić, Z. Weak ergodicity breaking from quantum many-body scars. *Nat. Phys.* **14**, 745-749 (2018).
- [47] Kaufman, A. M., Tai, M. E., Lukin, A., Rispoli, M., Schittko, R., Preiss, P. M. & Greiner, M. Quantum thermalization through entanglement in an isolated many-body system. *Science* **353**, 794-800 (2016).
- [48] Neyenhuis, B. et al. Observation of prethermalization in long-range interacting spin chains. *Sci. Adv.* **3**, e1700672 (2017).
- [49] Luitz, D. J., Laflorencie, N. & Alet, F. Many-body localization edge in the random-field Heisenberg chain. *Phys. Rev. B* **91**, 081103(R) (2015).
- [50] Wahl, T. B., Pal, A. & Simon, S. H. Signatures of the many-body localized regime in two dimensions. *Nat. Phys.* **15**, 164-169 (2019).
- [51] Altman, E. Many-body localization and quantum thermalization. *Nat. Phys.* **14**, 979-983 (2018).
- [52] Guo, Q. et al. Observation of energy resolved many-body localization. ArXiv: 1912.02818.
- [53] Potter, A. C., Morimoto, T. & Vishwanath, A., Classifi-

- cation of Interacting Topological Floquet Phases in One Dimension. *Phys. Rev. X* **6**, 041001 (2016).
- [54] Else, D. V., Monroe, C., Nayak, C. & Yao, N. Y. Discrete Time Crystals. ArXiv:1905.13232.
 - [55] Cazalilla, M. A., Citro, R., Giamarchi, T., Orignac, E. & Rigol, M. One dimensional bosons: From condensed matter systems to ultracold gases. *Rev. Mod. Phys.* **83**, 1405-1466 (2011).
 - [56] Cramer, M., Flesch, A., McCulloch, I. P., Schollwöck, U. & Eisert, J. Exploring Local Quantum Many-Body Relaxation by Atoms in Optical Superlattices. *Phys. Rev. Lett.* **101**, 063001 (2008).
 - [57] Guo, Q. et al. Dephasing-Insensitive Quantum Information Storage and Processing with Superconducting Qubits. *Phys. Rev. Lett.* **121**, 130501 (2018).
 - [58] Bardarson, J. H., Pollmann, F. & Moore, J. E. Unbounded Growth of Entanglement in Models of Many-Body Localization. *Phys. Rev. Lett.* **109**, 017202 (2012).
 - [59] Nandkishore, R. & Huse, D. A. Many-body Localization and Thermalization in Quantum statistical Mechanics. *Ann. Rev. Condens. Matter Phys.* **6**, 15-38 (2015).

Supplementary Note 1. The dynamics of tripartite mutual information for different initial states with identical energy density

We present several additional results supporting the main text. We first plot the energy density of isotropic initial states $|\theta, \phi, +\rangle$, defined as $\epsilon(\theta, \phi) \equiv (\langle \theta, \phi, + | H_{\text{Ising}} | \theta, \phi, + \rangle - E_{\min}) / (E_{\max} - E_{\min})$ in the θ - ϕ plane in Fig. 6a. We then benchmark the dynamics of tripartite mutual information (TMI) for different initial states $|\theta, \phi, +\rangle$ with the same randomly chosen ϵ , and the results are shown in Fig. 6b and c. It is seen that the saturated values of TMI are approximately equal to each other, if the energy densities are identical.

Next, we calculate the energy density of $|\theta, \phi, +\rangle$ in the superconducting qubit array, i.e., the Hamiltonian (8) in the main text. The results are depicted in Fig. 7a, showing that the energy density $\epsilon < 0.3093$ are not attainable for isotropic initial states. Thus, we consider another type of initial states, i.e., the Néel-type initial states

$$|\psi_0\rangle = |\text{GHZ}\rangle_{A1} \otimes |\theta_2, \phi_2, -\rangle \otimes |\theta_3, \phi_3, +\rangle \otimes \dots \otimes |\theta_{N-1}, \phi_{N-1}, +\rangle \otimes |\theta_N, \phi_N, +\rangle \quad (14)$$

with $\theta_i = \theta$, $\phi_i = \phi$ ($i = 1, 2, \dots, N$) and the number of qubits N as a even number for convenience. We further calculate the energy density of the Néel-type initial states with $\phi = 0$ and several values of θ . As shown in Fig. 7b, the dynamics of TMI for the initial states with $\epsilon < 0.3093$ are available by choosing the Néel-type initial states.

Figure 6b and c suggest that for the isotropic state, the saturated value of TMI is directly dependent on the ϵ . Therefore, it can be predicted that the saturated value of TMI is insensitive to the specific initial states, i.e., the isotropic or Néel-type states, if the ϵ of the states are equal to each other. The results in Fig. 8 and 9 provide further evidence for this prediction.

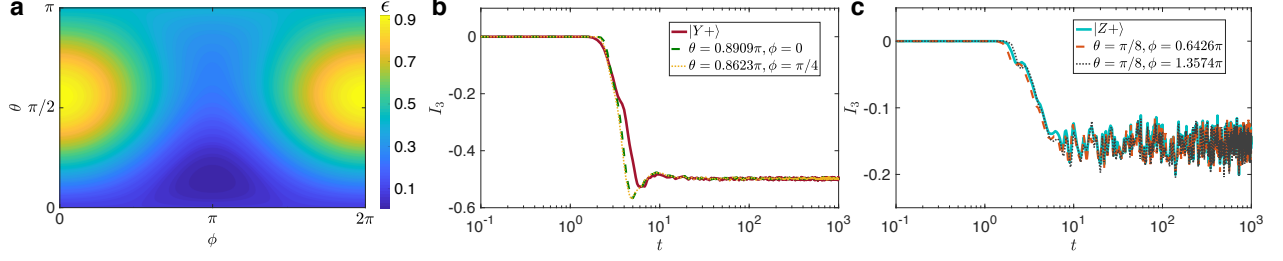


FIG. 6. **a** The energy density ϵ as a function of θ and ϕ in the non-integrable Ising model studied in the main text. **b** The quench dynamics of TMI with different isotropic initial states with the same energy density $\epsilon = 0.5602$. **c** is similar to **b** but with another energy density $\epsilon = 0.0812$.

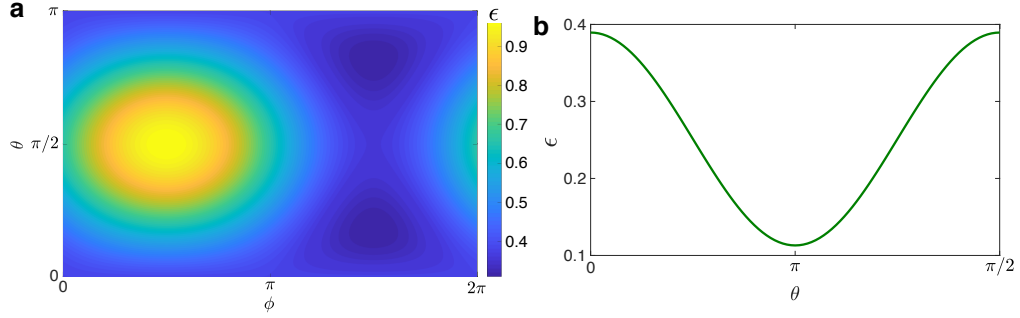


FIG. 7. **a** The energy density ϵ of isotropic initial states as a function of θ and ϕ in the superconducting qubit array studied in the main text. **b** The energy density ϵ of Néel-type initial states as a function of θ with $\phi = 0$.

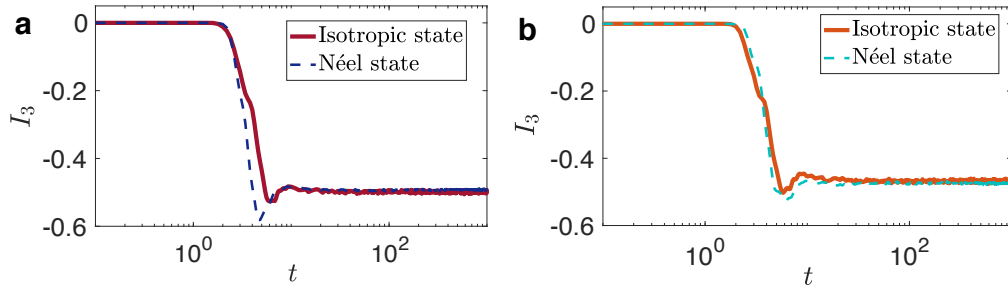


FIG. 8. **a** In the non-integrable Ising model, the dynamics of TMI I_3 for the isotropic initial state $|Y+\rangle$ and the Néel-type initial state with $\theta = \pi/2$. The value of energy density for both initial states is $\epsilon = 0.5602$. **b** The dynamics of I_3 for the isotropic initial state $|\theta = 0.5\pi, \phi = 0.4\pi\rangle$ and the Néel-type initial state with $\theta = 0.7013\pi$. The value of energy density for both initial states is $\epsilon = 0.6690$.

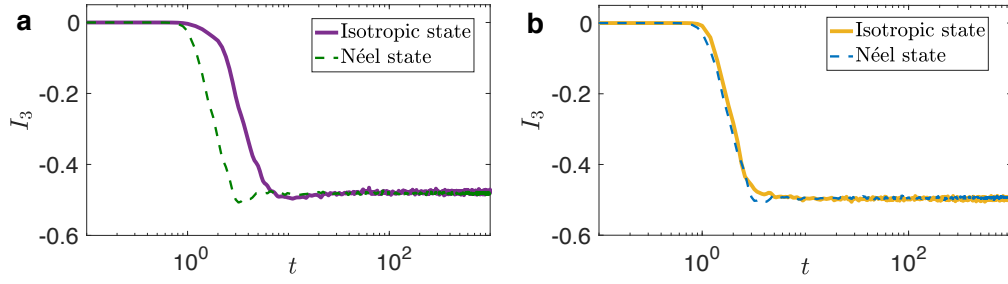


FIG. 9. **a** In the superconducting qubit array, the dynamics of TMI I_3 for the isotropic initial state $|\theta = 0.18\pi, \phi = 1.5\pi\rangle$ and the Néel-type initial state with $\theta = 0.1810\pi$. The value of energy density for both initial states is $\epsilon = 0.3093$. **b** The dynamics of I_3 for the isotropic initial state $|\theta = 0.4\pi, \phi = 1.5\pi\rangle$ and the Néel-type initial state with $\theta = 0.1124\pi$. The value of energy density for both initial states is $\epsilon = 0.3564$.

Supplementary Note 2. Non-equilibrium properties of the superconducting qubit array with the initial state $|Z+\rangle$

It can be directly calculated that for the superconducting qubit array considered in the main text, the inverse temperature of the initial state $|Z+\rangle$ is $\beta = 0$. Hence, $|Z+\rangle$ lies in the strong thermalization regime. In the main text, we have shown that the β of initial state $|\pi/2, 1.369\pi\rangle$ is also equal to 0. Here, we present a comparison between the dynamics of TMI with the initial state $|\pi/2, 1.369\pi\rangle$ and $|Z+\rangle$ in Fig. 10a, which is consistent with the results in Fig. 6, 8 and 9.

Moreover, we depict the time evolution of local observables with the initial state $|Z+\rangle$ in Fig. 10b. The dynamical behaviors of local observables are similar to those in the Fig. 4a of the main text. With the number of qubit $N = 14$, $\langle\sigma^\alpha(t)\rangle - \langle\sigma^\alpha\rangle_{\text{th}}$ ($\alpha \in \{x, z\}$) fast tend to 0 after relaxation. However, $\langle\sigma^y(t)\rangle - \langle\sigma^y\rangle_{\text{th}}$ suffers from a stronger finite-size effect. We then present the results of $\langle\sigma^y(t)\rangle - \langle\sigma^y\rangle_{\text{th}}$ with larger N in Fig. 10c. With the increase of N , the value of $\langle\sigma^y(t)\rangle - \langle\sigma^y\rangle_{\text{th}}$ becomes closer to 0.

Supplementary Note 3. A finite-size analysis of the no thermalization regime

The no thermalization regime in the non-integrable Ising model has been numerically revealed using the ma-

trix product state (MPS) algorithm that can simulate infinite quantum systems. A characteristic of the no thermalization regime is that the dynamics of local observables depart from their thermal values. For instance, in the non-integrable Ising model, with the initial state $|X+\rangle$, the dynamics of the local observable $\langle\sigma^x(t)\rangle$ does not converge to the thermal value $\langle\sigma^x\rangle_{\text{th}}$ (please see Ref. [29] and [30] for more details).

Here, we present the numerical results of the local observable $\langle\sigma^x(t)\rangle$ with finite system size N in the non-integrable Ising model in Fig. 11a. It is seen that the signature of no thermalization regime suffers from strong finite size effect. The approximately monotonous increase of $\langle\sigma^x(t)\rangle$ after the relaxation observed in the infinite system is interrupted by the obvious oscillations marked by the arrows in Fig. 11a. We recognize that the oscillations are dependent on the system size N . As a reasonable shortcut, we can study the location of the first dramatic cusp t_{cusp} marked by the arrows in Fig. 11a as a function of N , and the results are presented in Fig. 11b. Up to the system size $N = 24$, we show that $t_{\text{cusp}} \propto N$. Thus, for infinite system with $N \rightarrow \infty$, $t_{\text{cusp}} \rightarrow \infty$, and the obvious oscillation can not occur with finite time in the infinite system. We believe the finite-size analysis of the no thermalization regime is consistent with the MPS results shown in Ref. [29] and [30].

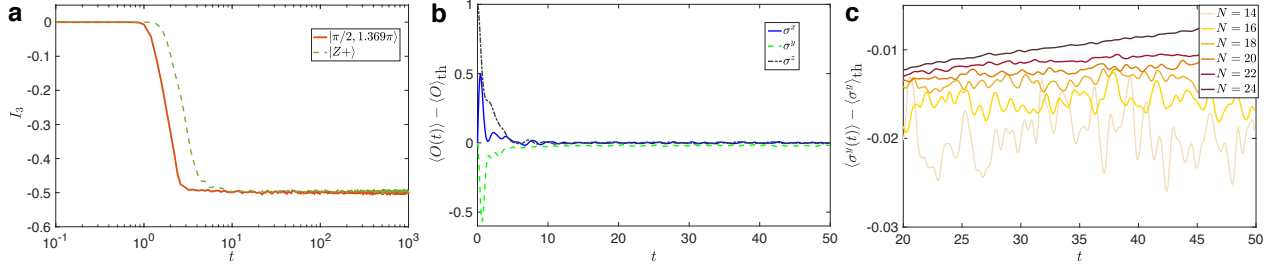


FIG. 10. **a** The dynamics of TMI with the initial state $|\pi/2, 1.369\pi\rangle$ and $|Z+\rangle$, whose stationary value is close to each other. **b** The dynamics of local observables with $N = 14$ and the initial state $|Z+\rangle$. **c** The dynamics of a local observable $\langle \sigma^y(t) \rangle - \langle \sigma^y \rangle_{\text{th}}$ with different N .

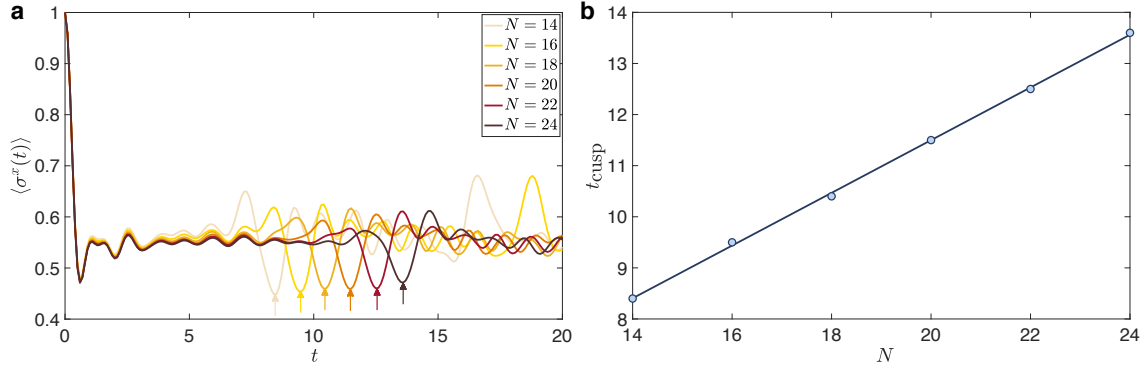


FIG. 11. **a** The dynamics of $\langle \sigma^x(t) \rangle$ in the non-integrable Ising model with the initial state $|X+\rangle$ and different system size N . **b** The dependence of t_{cusp} and N .